Kinetic coefficients for d-band metals in two-temperature states created by femtosecond laser irradiation

Kirill P. Migdal[a], Yurii V. Petrov[b], and Nail A. Inogamov[b]

[a]All-Russia Research Institute of Automatics, Rosatom, Moscow 127055, Russia;
[b]L. D. Landau Institute for Theoretical Physics, Russian Academy of Sciences, Chernogolovka 142432, Moscow region, Russia

ABSTRACT

Two-temperature thermal conductivity coefficient κ and electron-ion coupling parameter α are obtained using Boltzmann kinetic equation in the relaxation time approximation. These coefficients are necessary for the quantitative description of the two-temperature state with hot electrons $T_e \gg T_i$ created as result of absorption of femtosecond laser pulse. Simple, noble, and transition metals are considered. An influence of d-band electrons, which play a significant role, has been evaluated for two latter groups of metals.

Keywords: Ultrashort laser pulse, two-temperature state, transport coefficients

1. INTRODUCTION

There is a long list of technologically important applications based on femtosecond (fs) lasers. They are LIFT, laser pinning, laser colorizing, laser surface structuring, PLD, MAPLE, biomedical applications, and so on*. Those applications are connected with micro machining and with moderate energy depositions into target - absorbed fluences F_{abs} are in the range 20-1000 mJ/cm^2. In this range interatomic forces and cohesive properties are significant. This is an area of material research sciences. Another range of applications, just mentioned for completeness, is based on high intensities regimes from 10^{16} to 10^{18} W/cm^2 and even higher - to 10^{21} W/cm^2 - a limit achieved at modern petawatt laser facilities. Those high field applications are: plasma plume with highly charged ions; K_α X-ray sources; hard Bremsstrahlung X- and γ-ray sources; plasma mirror and HHG (high harmonics generation); electron, proton, ^{12}C, and other ions acceleration to $\sim$0.1-1 GeV. Another directions of recent developments on fs and ps laser-matter interaction are connected with very high repetition rates $\sim$ 100 MHz; with studies of plasmonic effects on rough surfaces†; and with delivery of a pulse on a workpiece by robotic system equipped with a fiber laser device.

A heart of micro machining technologies is a two-temperature (2T) stage $T_e \gg T_i$ created by absorption of energy by electron subsystem. Subsequent thermal and mechanical stages follow the 2T stage. Striking is that the existence of laser induced 2T states[1] was proposed many years before the first fs laser-matter experiments.[2–4]

Experiments[2–4] have been conducted at small absorbed fluences F_{abs} - targets remain in solid state. For fs micro machinery the metal has to be molten or even ablated; melting threshold F_m is below ablation threshold F_{abl} for short laser pulses; $F_{abs}|_{abl} \sim 50 - 200$ mJ/cm^2 for different metals. Maximum pressures and electron temperatures for those energy depositions are $10 - 50$ GPa and $1 - 3$ eV. Below the kinetic coefficients will be calculated for this energy range. To consider ablation, the hydrodynamical effects should be included. Corresponding system of equations is

$$\rho(x^0,t)\frac{\partial x(x^0,t)}{\partial x^0} = \rho^0, \quad \rho^0\frac{\partial u}{\partial t} = -\frac{\partial P(x^0,t)}{\partial x^0}, \quad \frac{\partial x(x^0,t)}{\partial t} = u(x^0,t), \tag{1}$$

Further author information: (Send correspondence to N.A.I.)
N.A.I.: E-mail: nailinogamov@gmail.com, Telephone/fax: +7 495 702 9317

*LIFT, PLD, MAPLE are abbreviations: laser induced forward transfer, pulsed laser deposition, and matrix assisted pulsed laser evaporation; see introductional descriptions in Wikipedia

†Plasmons are absent in case of well polished surface and in case of excitation by X-ray light.

Fundamentals of Laser-Assisted Micro- and Nanotechnologies 2013, edited by Vadim P. Veiko, Tigran A. Vartanyan,
Proc. of SPIE Vol. 9065, 906503 · © 2013 SPIE · CCC code: 0277-786X/13/$18 · doi: 10.1117/12.2053172

$$\rho^0 \frac{\partial(E_e/\rho)}{\partial t} = -\frac{\partial q}{\partial x^0} - \frac{\rho^0}{\rho}\alpha \cdot (T_e - T_i) + \frac{\rho^0}{\rho} Q - P_e \frac{\partial u}{\partial x^0}, \quad q = -\frac{\rho\kappa}{\rho^0} \frac{\partial T_e}{\partial x^0}, \tag{2}$$

$$\rho^0 \frac{\partial(E_i/\rho)}{\partial t} = \frac{\rho^0}{\rho}\alpha \cdot (T_e - T_i) - P_i \frac{\partial u}{\partial x^0}, \quad Q = \frac{F_{abs}}{\sqrt{\pi}\,\tau_L\,\delta} \exp\left(-\frac{t^2}{\tau_L^2}\right) \exp\left(-\frac{x}{\delta}\right) \theta(x). \tag{3}$$

Expressions (1-3) correspond to conservation laws for mass, momentum, and energy together with necessary definitions of Lagrangian trajectory $x(x_0, t)$, Lagrangian coordinate is x_0, $x(x_0, t = -\infty) = x_0$, an axis x is perpendicular to the plane surface; spatially one-dimensional case is considered. Q is an energy source; duration of pump laser pulse is τ_L, skin depth is δ. Time is counted from arrival of the laser pulse maximum, while the origin of spatial coordinate x is placed on an initial position of a frontal surface of film; $\theta(x) = 1, x > 0$, $\theta(x) = 0, x < 0$; initially metal locates at the right side $x > 0$ relative to initial position of a surface.

Thermodynamic functions $E_e(\rho, T_e, T_i)$, $E_i(\rho, T_e, T_i)$, $P(\rho, T_e, T_i)$, $P_e(\rho, T_e, T_i)$, $P_i(\rho, T_e, T_i)$ (2T-EOS, equation of state) and kinetic coefficients κ and α are needed[5–7] to solve system (1-3) of 2T hydrodynamics (2T-HD). Expression for pressures may be omitted in the case without motion $x(x_0, t) \equiv x_0$. As was said, in this paper we will focus on coefficients κ and α. Description of 2T-EOS will be given elsewhere. Some results about 2T-EOS are presented in paper.[8] We use one-parabolic approximation of electron spectrum for simple (one-band) metals, and two-parabolic approximation for noble and transition metals, where two bands (s and d) exist. This is an effective description, it allows us to consider interaction as collisions between particles with effective masses m_{eff}. DFT (density functional theory) simulations were used to calculate band structure and to find m_{eff} and edges of bands. Significant complication of calculations is connected with an upper edge of a d-band; s-band continues to infinity. We separate total density of electron states (DOS) g into partial DOS for the s- and d-bands (g_s and g_d) to define masses m_{eff} of s- and d-electrons. The paper[9] presents approach when collision integrals are calculated without approximation of dispersion relations by effective masses m_{eff}. In[9] total DOS $g = g_s + g_d$ is used, similar to paper.[10] It is not possible to separate s- and d-bands in this approach, see comparisons and discussion in paper.[6]

2. BAND STRUCTURE ACCORDING TO DFT AND ITS APPROXIMATION

Calculations of spectra is based on DFT simulations performed using VASP code.[11] Example of simulations in case of copper is shown in Fig. 1. The code allows to separate s,p- and d-bands with satisfactory accuracy. Table 1 presents parameters of two-parabolic approximation of the DFT DOS spectra.[6] Two upper bands (s,p and d - $3d^{10}4s^1$) of Cu are quantized in the DFT approximation. The bands below those valence bands are described by the PAW LDA pseudopotential with a plane-wave cutoff 500 eV, 21*21*21 k-points and 25 electron bands. The bottom bands are separated by a wide gap $\Delta > 50$ eV from the $3d^{10}4s^1$ shells. Therefore an approximation with a PAW LDA pseudopotential is applicable in our range of electron temperatures $T_e \ll \Delta$. Pseudopotential Cu-pv is taken from the VASP library is used to estimate value Δ. The Cu-pv potential includes a 3p-shell.

Table. 1. Parameters of two-parabolic approximation of normal density, cold DFT DOS. Those values minimize an average square deviation between DFT DOS and two-parabolic spectra

Metal	ε_s, eV	ε_1, eV	ε_2, eV	z_s	z_d	m_s, m_e	m_d, m_e
Al	-11.06	-	-	3	-	1.05	-
Au	-8.33	-7.18	-1.83	1.5	9.5	0.87	4.64
Cu	-10.02	-5.59	-1.65	1.75	9.25	1.02	7.85
Fe	-9.4	-5.5	0.77	1	7	0.75	4.68
Ni	-8.8	-5.0	0.17	1.5	8.5	1.10	6.15
Pt	-10	-7.5	0.2	1.5	8.5	0.78	3.31
Ta	-8	-4.6	1	2	3	1.05	2.39

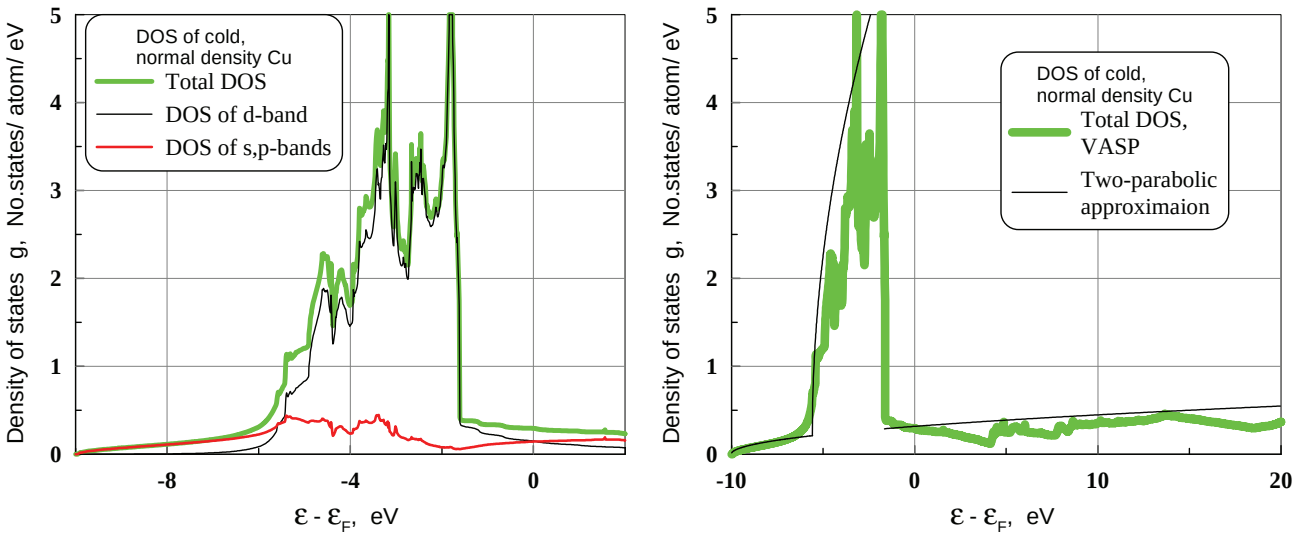

Figure 1. *Left panel.* Total g and partial g_s, g_d DOS of cold, normal density copper. *Right panel.* Comparison of a total DOS with its two-parabolic approximation $g = g_s + g_d$; $g_i = (\sqrt{2}/\pi^2) m_i^{3/2}/n_{at}/\hbar^3 \sqrt{\varepsilon - \varepsilon_i}$; $i =$ s or d, n_{at} is an atomic concentration, ε_i is ε_s for s-electrons, and ε_1 for d-electrons; ε_s and ε_1 are the bottom edges for s- and d-electrons, resp. It is suggested that s-band exist at $\varepsilon > \varepsilon_s$, while the d-band occupies a range $\varepsilon_1 < \varepsilon < \varepsilon_2$.

Copper in our calculations is considered as a fcc crystal with a lattice period 0.35208 nm at normal density $V/V_0 = 1$, $V = 1/\rho$. In a point V_0 on a V-axis the calculated total pressure changes a sign. Influence of 3D isotropic expansion or compression of cold crystal onto total DOS is studied. We consider isotropic deformations from $V/V_0 = 0.5$ to $V/V_0 = 2$. Results are shown in Fig. 2 (left). Total DOS for every density in Fig. 2 (left) is plotted against a Fermi level $\varepsilon_F(V; T_e = 0)$ for Cu defined by equation:

$$\int_A^B g(\varepsilon; V; T_e = 0) d\varepsilon = 11, \quad A = \varepsilon_s(V; T_e = 0), \quad B = \varepsilon_F(V; T_e = 0), \tag{4}$$

specific for this particular density. A definition of Fermi energy is generalized for arbitrary temperatures T_e :

$$\int_A^B g(\varepsilon; V; T_e) d\varepsilon = 11, \quad A = \varepsilon_s(V; T_e), \quad B = \varepsilon_F(V; T_e), \tag{5}$$

since total DOS $g(\varepsilon; \rho, T_e)$ is temperature depended. Equation defining chemical potential $\mu(\rho, T_e)$ is

$$\int_A^B f\, g(\varepsilon; V; T_e) d\varepsilon = 11, \quad A = \varepsilon_s(V; T_e), \quad B = \mu(V; T_e), \quad f = \{1 + \exp[(\varepsilon - \mu)/k_B T_e]\}^{-1}, \tag{6}$$

where f is Fermi distribution function. Of course, roots $\varepsilon_F(V; T_e)$ and $\mu(V; T_e)$ of equations (5) and (6) differs. Those roots coincide at zero temperature $T_e = 0$: $\varepsilon_F(\rho, T_e = 0) \equiv \mu(\rho, T_e = 0)$. In the equations (4-6) we use ε_s as a bottom limit of an integration range since the edge ε_s is less than the edge ε_1, see Table 1. We see that cold spectra in Fig. 2 (left) varies with density, see also.[12,13] A d-band becomes more narrow with stretching. But even at the highest considered here stretching $V = 2V_0$ a cold copper remains metal - there is no gap at a Fermi level.

Changes of total g and partial g_s, g_d DOS under variation of electron temperature T_e are investigated, see Fig. 2 (right) and Figs. 3. A range of electron temperatures is from 1 kK to 55 kK. Similar researches but without partial DOS have been performed in papers.[13–16] The bottom edge of spectrum ε_s is defined by the edge of the s-band. It is insensitive to increase of electron temperature, see Fig. 2 (right) and Fig. 3 (right). But the d-band is influenced by temperature T_e, see Figs. 4. The bottom ε_1 and the upper ε_2 edges are shifted

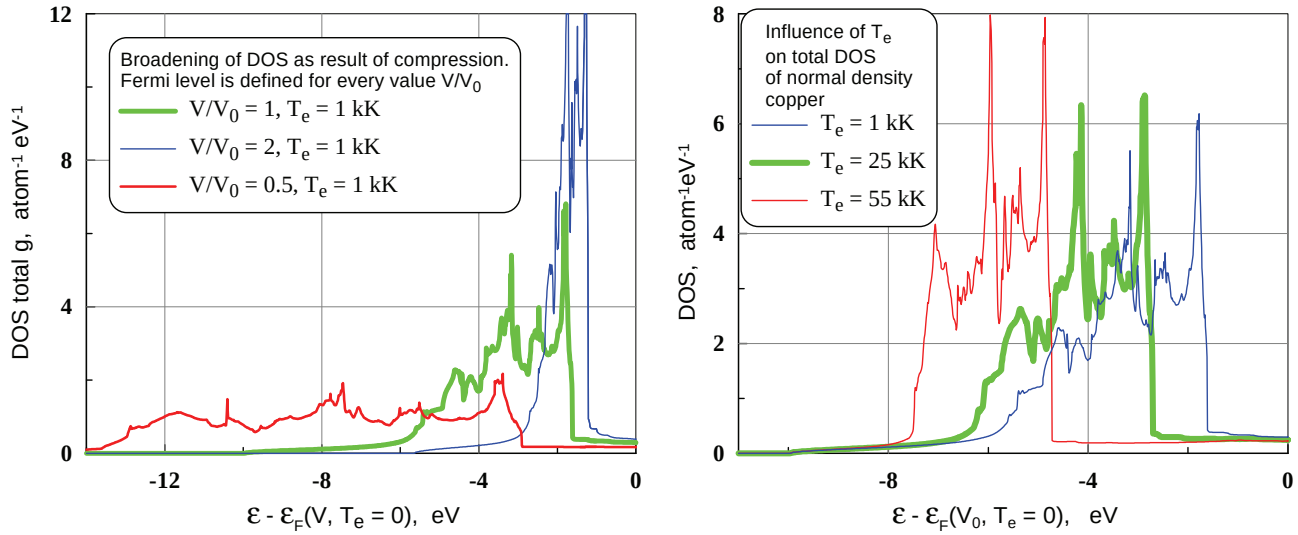

Figure 2. *Left panel.* Deformation of total electron spectra with variation of density of cold Cu. We call cold Cu (" $T_e = 0$ ") the case with low temperature $T_e = 1$ kK. It is approximately the same as the case $T_e = 0$. An absorption cutoff $\varepsilon_F(V, T_e = 0) - \varepsilon_2(V, T_e = 0)$ becomes larger as density increases (a shift into UV side). *Right panel.* Deformation of total electron spectra with variation of electron temperature T_e of normal density Cu. We see that the bottom edge ε_s is uninfluenced (!) by heating of electrons. This is better seen in Fig. 3 (right) below.

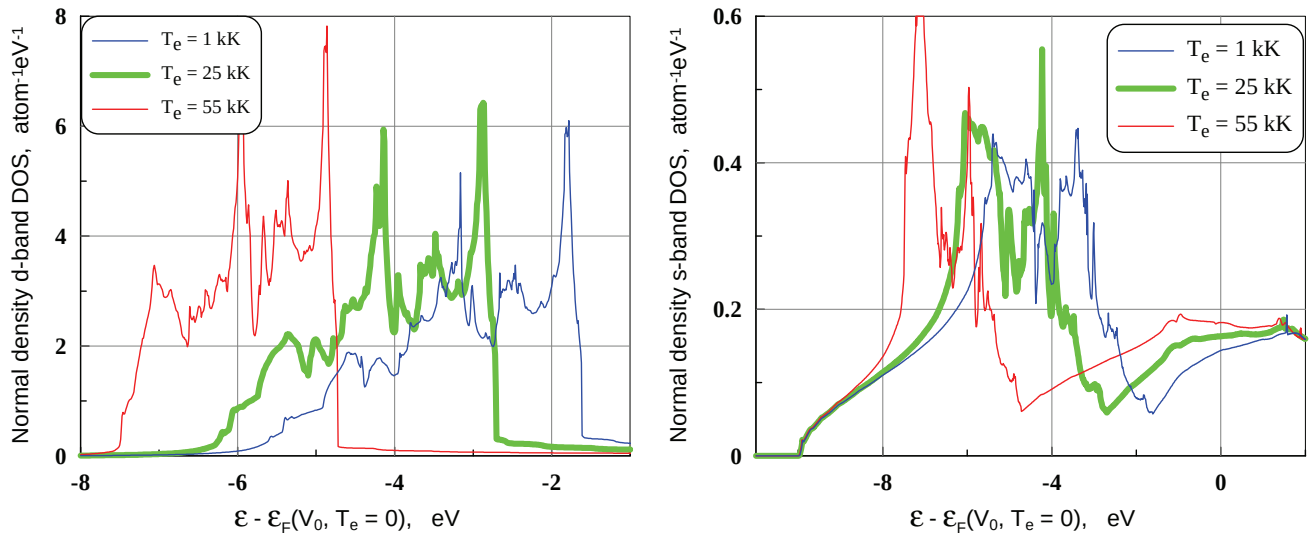

Figure 3. *Left panel.* Variation of a d-band $g_d(\varepsilon, T_e)$ with temperature T_e. *Right panel.* Variation of a s-band $g_s(\varepsilon, T_e)$ with temperature T_e. The spectra deform while the left edge ε_s remains unchanged!

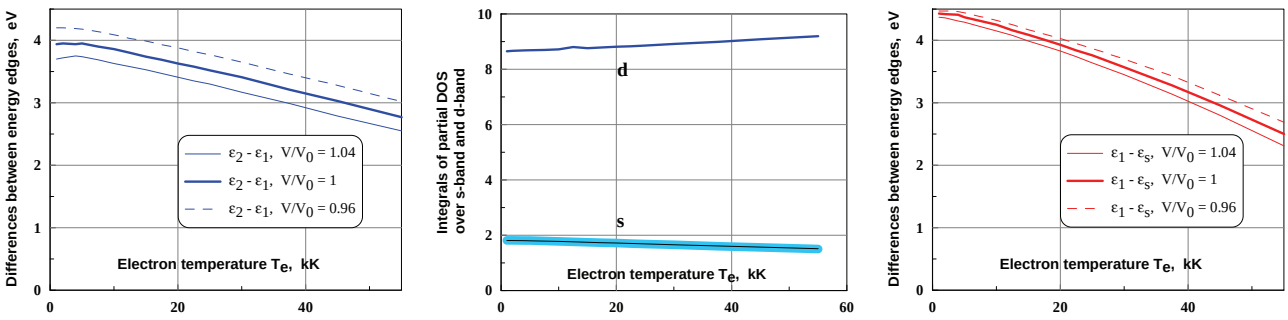

Figure 4. *Left panel.* Shrinking of d-band as temperature T_e increases. Width of d-band $\Delta_d(\rho, T_e) = \varepsilon_2 - \varepsilon_1$ as function of density and temperature T_e is plotted. A width Δ_d increases at fixed T_e when Cu becomes denser (V/V_0 becomes smaller). Variations of ρ ($\pm 4\%$) and T_e (1-55 kK) cover a range typical for 2T stage and fluences F_{abs} of the order of ablation threshold. Corresponding pressure changes are from -6 GPa to 8 GPa in this $\pm 4\%$ interval of 3D isotropic spatial deformations. *Middle panel.* Temperature dependencies of integrals $\tilde{z}_i(\rho, T_e) = \int_a^b g_i(\rho, T_e) d\varepsilon$ characterizing capacity of partial bands; here $i =$ s or d, $a_s = \varepsilon_s(\rho, T_e)$, $b_s = \varepsilon_F(\rho, T_e)$ according to definition (5), $a_d = \varepsilon_1(\rho, T_e)$, $b_d = \varepsilon_2(\rho, T_e)$. Those integrals are taken over ranges corresponding to a part of s-band and for whole d-band. They characterize density and temperature T_e depended modifications of partial spectra. Density modifications $\pm 4\%$ are negligible - there are three curves marked "s", they correspond to three values of compression $V/V_0 = 0.96, 1, 1.04$. We see that in a scale of picture those three curves, plotted by lines of different thickness and color, merge into one curve. *Right panel.* A bottom of the d-band ε_1 descends as temperature T_e grows, see Fig. 3 (left). While a bottom of s-band is insensitive to electron temperature increase, see Fig. 3 (right). Therefore an energy interval between those bottoms, plotted here, drops down as temperature T_e increases. We see that density and temperature variations during 2T stage moderately deform electron spectra obtained thanks to DFT. Hence, a two-parabolic approximation of the DFT DOS also changes moderately during 2T stage. This is a base for using of the two-parabolic DOS taken at zero electron temperature $T_e = 0$ in our calculations of kinetic coefficients below.

down, and width $\varepsilon_2 - \varepsilon_1$ shrinks, see Figs. 4. A middle part of the s-band in Fig. 3 (right) changes with T_e, perhaps as result of hybridization with d-electrons and changes in the d-shell.

Isotropic deformations keep a symmetry of a lattice. A fcc cubic cell containing four atoms is used in DFT calculations. A cubic cell fulfills 3D periodic boundary conditions. VASP[11] calculations of DOS is performed in two stages (we follow here to kind advice given to us by V.V. Stegailov). On the first stage the charge density is obtained for a smearing parameter in a Fermi-Dirac distribution corresponding to the chosen electron temperature T_e. At the second stage the fixed charge density, obtained at the first stage, is used for not self-consistent calculation of DOS. The second stage calculations are performed using tetrahedron method with Bloechl corrections. Thermodynamic quantities (total energy and pressure) are taken from the first stage. Total DOS, obtained at the second stage, depending on T_e and V/V_0, is decomposed onto separate partial contributions from s- and d-bands. The results of such decomposition for cold, normal density $V/V_0 = 1$ Cu is shown in Fig. 1 (left). Decomposition for elevated temperatures T_e is presented in Figs. 3.

As was said in captions to Fig. 4, in the range of compressions $V/V_0 = 0.96 - 1.04$, characteristic for 2T stage, variations of parameters of the two-parabolic approximation (ε_i, z_i and effective masses, see Table 1) are minimal. Increase of temperature T_e up to several eV is more significant, but corresponding changes are also moderate (see Fig. 4) in case of noble metals, when ε_2 is negative and d-band is located below the zero temperature Fermi level (4). Significant changes with increase of T_e take place in transition metals ($\varepsilon_2 > 0$), especially in nickel and platinum where a value ε_2 is small, and density of d-states at Fermi level (4) is very large, see.[7] In next Section influence of variation of the two-parabolic parameters due to changes in temperature T_e is estimated in case of copper.

3. THERMODYNAMICS OF COPPER IN TWO-TEMPERATURE STATE

Heating of electron subsystem significantly influences thermodynamic characteristics. E.g., pressure increases from zero value at fixed normal density as temperature T_e increases from a room temperature value 300 K;

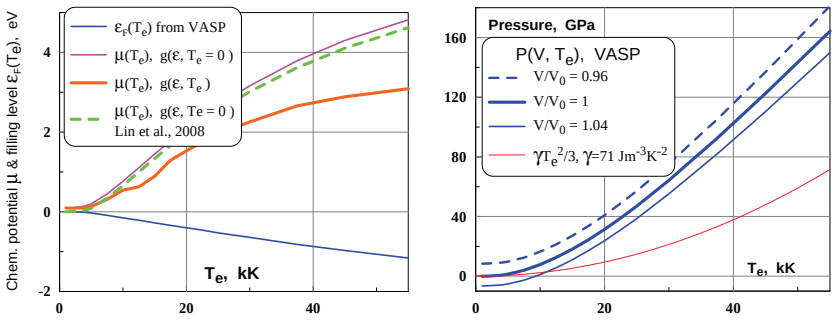

Figure 5. *Left panel.* The bottom curve corresponds to a filling level $\varepsilon_F(T_e)$ (5) taken directly from VASP simulations at different temperatures T_e. The integral (5) gives a level where total DOS accumulates number of states which equals to 11. The level $\varepsilon_F(T_e)$ descends down since a total DOS $g(\varepsilon, T_e)$ is shifted down as temperature T_e increases, see Fig. 2 (right). Chemical potential demonstrates opposite behavior. If DOS $g(\varepsilon)$ decreases around Fermi level $\varepsilon_F(\rho, T_e = 0)$ for higher values ε then function $\mu(T_e)$ increases with temperature in the temperature range is of the order of several eV. For large T_e the function $\mu(T_e)$ decreases for any DOS since degeneracy effects become small. There is an interplay of small positive and large negative gradients $\partial g/\partial\varepsilon$ around the level $\varepsilon_F(\rho, T_e = 0)$. In small vicinity the gradient $\partial g/\partial\varepsilon$ may be positive, while in the wider vicinity the strong drop of DOS at the edge ε_2 of a d-band becomes important. Mainly this drop defines the rising behavior of a function $\mu(T_e)$. In our case with Cu, this drop is more important than the effect connected with the shift down of DOS $g(\varepsilon, T_e)$ in Fig. 2 (right) as T_e increases. *Right panel.* Heating of electrons rises pressure of 2T solid copper. Classical dependence (red curve) with a theoretical value γ significantly underestimate pressure since contribution to pressure as a result of liberation of electrons from a d-band is not included. Value $\gamma = 71\ \mathrm{J\,m^{-3}\,K^{-2}}$ corresponds to small temperatures T_e when a d-band is insignificant.

normal density is defined at 300 K. Dependence of chemical potential $\mu(T_e)$ is important for calculations of transport coefficients (electrical and thermal conductivities σ, κ) and coupling parameter α, see eqs. (2,3). Therefore here we shortly present results of our calculations concerning 2T equation of state. Functions $\mu(\rho, T_e)$ are shown in Fig. 5 (left). We suppose that ions are fixed in their lattice positions in our DFT electron temperature dependent calculations. Fig. 5 (left) illustrates differences between different methods of calculation of chemical potential. The curve $\mu(V/V_0 = 1, T_e)$ marked " $g(T_e)$ " is found by solving Eq. (6) with temperature dependent DOS $g(\varepsilon; V = V_0, T_e)$ shown in Fig. 2 (right). While the curve $\mu(V/V_0 = 1, T_e)$ Fig. 5 (left) marked " $g(T_e = 0)$ " is found by solving Eq. (6) with a DOS $g(\varepsilon; V = V_0, T_e = 0)$ corresponding to zero temperature ("cold spectrum"). The same calculation with a cold spectrum has been made in paper.[10] This is the curve "Lin et al., 2008" in Fig. 5 (left). It agrees well with our calculation (curve " $g(T_e = 0)$ "). Difference between the curves " $g(T_e)$ " and " $g(T_e = 0)$ " in Fig. 5 (left) means that temperature deformations of electron spectra of Cu are considerable, see also discussion around Fig. 4.

Dependencies of energy and pressure are shown in Figs. 5 (right) and 6. In Fig. 6 (left) functions p and E are presented. A ratio p/E for the curves shown in Fig. 6 (left) is ≈ 0.8 with $\pm$ variations $\approx 5\%$ near an average value in the chosen range of temperatures T_e . The ratio is significantly less than Gruneisen parameter for metals (≈ 2) and higher than classical value 2/3 corresponding to Fermi gas. There is small influence of compression on dependence of energy on temperature T_e, see Fig. 6 (left). Shift of minimum of the dependence $E(\rho, T_e)$ for our density variations $(\delta\rho/\rho) \pm 4\%$ is very small, because the minimum corresponds to the point where pressure is zero and therefore variations of energy near minimum are variations of the second order $(\delta\rho/\rho)^2$. It is interesting that the volume energy density shown in Fig. 6 (left) depends on compression in the opposite direction in comparison with changes of pressure with compression - compressed state has larger pressure but slightly smaller energy.

In Fig. 6 (middle) the single-particle energies defined by single-particle spectrum, particle occupation numbers, and chemical potential are compared with energy taken directly from VASP simulation. There is double counting of electron-electron electrostatic energy included into single-particle spectrum. There is a strong shift down of a d-band with increase of electron temperature T_e, see illustration in Fig. 2 (right). This shift is so strong that the single-particle energies begin to decrease (!) with increase of temperature T_e. Therefore, of course, data obtained in the DFT approximation at elevated temperatures T_e should be treated with caution.

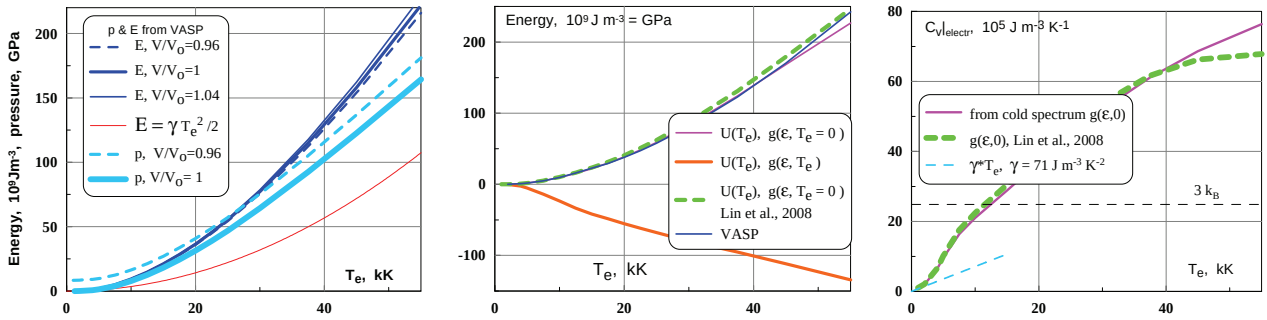

Figure 6. *Left panel.* Comparison of pressure and volume density of energy both taken from simulations done by VASP. Copper. In Mie-Gruneisen approximation the increase of energy due to heating of electron subsystem at fixed volume is represented by thermal contribution. There is a sum of two terms in Mie-Gruneisen approximation. They are a cold curve and a thermal contribution. We call the second term an electron thermal contribution since energy grows as result of heating of electrons while ions remain cold. *Middle panel.* Copper. Comparison of volume densities of energy calculated in three different ways: (i) $\int_{es}^{\infty} \varepsilon f[\varepsilon, \mu_1(T_e), T_e] g(\varepsilon, T_e = 0) d\varepsilon$, (ii) $\int_{es}^{\infty} \varepsilon f[\varepsilon, \mu_2(T_e), T_e] g(\varepsilon, T_e) d\varepsilon$, and (iii) are values taken from VASP; here μ_1 and μ_2 correspond to chemical potentials calculated based on cold DOS $g(\varepsilon, 0)$ or based on the temperature dependent DOS $g(\varepsilon, T_e)$, resp.; see in this respect Figs. 2 (right) and 5 (left). In Ref.,[10] marked as "Lin et al., 2008" here, the method (i) is used. The direct sums of single-particle energies weighted by the DOS and Fermi distribution are compared here with the internal energy taken from VASP simulation. There is a double counting of electron-electron electrostatic energy when calculating these direct sums, so they aren't true internal energy. *Right panel.* Removal of degeneracy and increase of heat capacity of copper as temperature T_e grows. In a gas limit an electron heat capacity is $11(3/2)k_B = 137 \cdot 10^5$ J m^{-3} K^{-1}.

It is interesting that in spite of double counting of electron-electron Coulomb interaction energy the energy based on cold single-particle spectrum is nicely correlated with VASP energies (agreement between the upper three curves in Fig. 6, middle).

4. ELECTRON-ION COUPLING PARAMETER

In our approach the calculations of electron-phonon coupling α for d-band metals are based on Lindhard approximation for dielectric permittivity in expression for Coulomb interaction operator, see the paper[6] and references given in this paper. For illustration the dependencies $\alpha(T_e)$ are shown in Figs. 7. They weakly depend from ion temperature T_i if this temperature is above Debye temperature. For tantalum values of electron-phonon coupling are almost independent from temperature T_e. For other metals these dependencies behave monotonously. If the right edge of a d-band ε_2 is positive (higher than $\mu(T_e = 0)$, see Table 1) then function $\alpha(T_e)$ decreases as temperature T_e grows. Metals with a negative edge $\varepsilon_2 < 0$ demonstrate opposite dependence, comp. Figs. 7 (left) and (right).

Fig. 7 (middle) is plotted to show an influence of variation of electron spectra with temperature T_e on coupling. Fig. 4 gives information concerning an amplitude of temperature dependencies of the two-parabolic parameters on T_e. Coupling is much less in case of noble metals in comparison with transition metals with small edge energy ε_2 when density of states is high on a Fermi surface (compare the left versus middle and right panels in Fig. 7). In Fig. 7 (right) the dependence of electron-phonon coupling from electron temperature for gold is shown. Case of gold is similar to the case of Cu (Fig. 7 middle). Noble metals behave qualitatively different from transition metals like Ni, Pt, and Fe. In noble metals the d-band contribution α_d increases with temperature, while in transition metals it goes down when temperature T_e increases. Roughly coupling is inversely proportional to ion mass. Energy transfer to ion subsystem through s-electrons dominates in case of noble metal at relatively small temperatures. This is clear from Fig. 7 (right). But a d-band introduces a main contribution to e-i energy transfer when d-electrons are presented in the window on an energy axis where degeneracy is thermally removed. Outside the temperature range $T_e \sim \varepsilon_2$ for transition metals the d-band contributions are in the order of magnitude the same for different metals. Let us mention that recent experiments[17] seems give smaller values (than shown in Fig. 7 right) $\approx 0.22 \cdot 10^{17}$ W m^{-3} K^{-1} for coupling

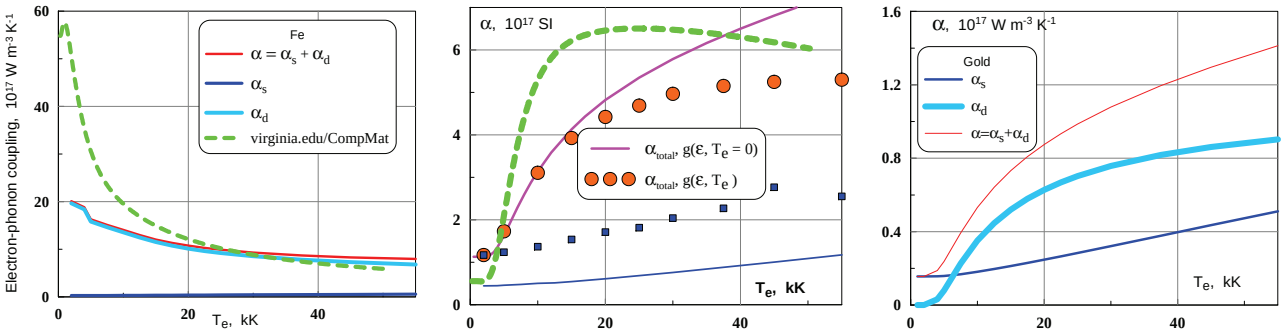

Figure 7. *Left panel.* Strong dependence of coefficient $\alpha(T_e)$ on temperature T_e in case of transition metals with small positive value of the edge energy ε_2, when d-band and s-band are mixed at the Fermi surface. Compare with similar results obtained recently[7] for resistivity of such metals in 2T state. Here the case of Fe is shown. Our approach allows to separate contributions of different bands into e-i coupling. We see that contribution of s-band is negligible in comparison with contribution from a d-band. Dashed line presents dependence taken from site http://www.faculty.virginia.edu/CompMat/ *Middle panel.* Dependencies $\alpha(T_e)$ for Cu and $\alpha_s(T_e)$ for Fe. There are five curves here. They correspond to: (i) calculations according to model[6] with parameters of a two-parabolic approximation taken from a cold DOS spectrum $g(\varepsilon, 0)$ (they are presented in Table 1). (ii) The same model but now for the first time we include dependence of the two-parabolic parameters on temperature T_e. This is the curve $g(\varepsilon, T_e)$. In this connection we have to say that Fig. 7 (left) for Fe is plotted for the case of a cold spectrum. (iii) Green dashed dependence $\alpha(T_e)$ for Cu are taken from the cited above site virginia.edu/CompMat/ (iv) Blue squares give a partial dependence $\alpha_s(T_e)$ for the temperature dependent parameters $g(\varepsilon, T_e)$. (v) Blue curve presents s-i coupling $\alpha_s(T_e)$ for Fe. It is taken from Fig. 7 (left). We see that an energy transfer rate through s-band is in the order of magnitude the same for Cu and Fe. The coupling $\alpha_s(T_e)$ weakly depends on T_e. *Right panel.* Partial α_s, α_d and total $\alpha = \alpha_s + \alpha_d$ coupling parameters for gold.

parameter of gold at elevated temperatures $T_e \sim 2$ eV. Variation of values α for Au is discussed in paper.[6] For smaller effective masses the values of our e-i coupling parameter drops down to values $\approx 0.5 \cdot 10^{17}$ W m^{-3} K^{-1} at temperatures $T_e \sim 2$ eV.

5. TWO-TEMPERATURE ELECTRON HEAT CONDUCTIVITY

Fig. 8 (left) shows dependence of 2T heat conductivity coefficient $\kappa(\rho, T_e, T_i)$ of copper on temperatures T_e and T_i. Our model[6] and two-parabolic parameters listed in Table 1 are used for calculations of two curves shown by continuous lines. Rather steep linear growth of conductivity κ at relatively small temperatures T_e is connected with increase of electron heat capacity with temperature T_e due to partial removal of degeneracy, see Fig. 6 (right). Electron-ion collision frequency ν_{ei} is fixed since ion temperature T_i is constant along the curve $\kappa(T_e)$ during this steep growth[‡], while the electron-electron collision frequency ν_{ee} is less than ν_{ei} up to the end of this piece of rather steep growth of conductivity. This growth ends when frequency ν_{ee} growing with T_e overcomes constant ν_{ei}. At small temperatures T_i even a maximum appears at the dependence of coefficient κ on T_e. At elevated temperatures T_i the steep growth decreases and the maximum is smeared out. Increase of frequency ν_{ee} with temperature T_e can not exceed the increase of heat capacity with temperature T_e, therefore growth of coefficient $\kappa(T_e)$ continues but with smaller slope. We see that at elevated electron temperatures the coefficient $\kappa(T_e)$ greatly exceeds its room temperature value. This is one of the two reasons[§] why a depth of heated layer d_T is several times larger than a skin depth δ.

Phenomenological expression "5/4" cited in caption to Fig. 8 (left) is

$$\kappa = C\,(\theta_e^2 + 0.16)^{5/4}(\theta_e^2 + 0.44)/\sqrt{\theta_e^2 + 0.092}/(\theta_e^2 + \beta\theta_i),$$

here temperatures are normalized to Fermi energy $\theta_e = k_B T_e/E_F$, $\theta_i = k_B T_i/E_F$. Coefficients C and β for Cu used to plot the three dashed curves in Fig. 8 (left) are taken from paper.[16] Expression "5/4" underestimate

[‡]This is not true for transition metals, see next Section.

[§]Another reason is connected with a finite duration of a two-temperature stage.

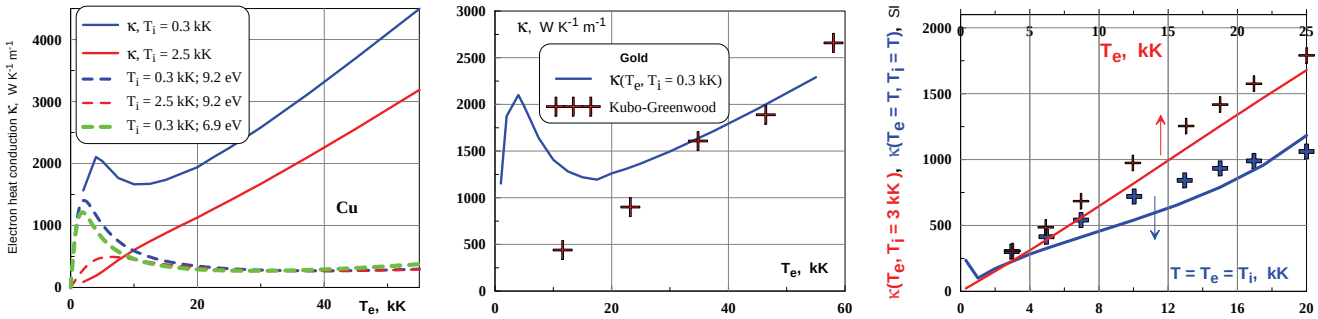

Figure 8. *Left panel.* Two continuous curves give a two-temperature heat conductivity of Cu according to model[6] at normal density $\rho_0 = 9$ g/cc. The conductivities given by a still popular phenomenological expression "5/4" are shown by thee dashed lines for comparison. The expression "5/4" is described in text. Two values connected with the dashed lines are ion temperature T_i and Fermi energy in [eV]. *Middle panel.* Comparison of our model with DFT MD and Kubo-Greenwood approach[18] in case of two-temperature solid gold. *Right panel.* Comparison of our model with DFT MD/Kubo-Greenwood approach in case of one-temperature $T_e = T_i = T$ (blue curves) and two-temperature $T_e > T_i = 3$ kK (red curves) molten aluminum.[19]

conductivity at high temperatures T_e since it overestimates frequency ν_{ee} written as $\nu_{ee} \propto T_e^2$ according to low temperature simple asymptote,[20] see discussion of this circumstance in paper.[21] Frequency ν_{ee} in expression "5/4" strongly exceeds e-i frequency at elevated values T_e. Therefore the dependencies "5/4" for different temperatures T_i merge into one curve. At smaller electron temperatures the expression "5/4" gives results qualitatively similar to the results from our model.

Nowadays DFT simulations are used to define quantum transport properties of liquids and solids. Simple[22] and transition metals[23,24] are considered. Those papers report ab-initio results concerning only one-temperature case. Recently first papers[18,19,25,26] appear dealing with two-temperature liquids (Al) and solids (Au). In these calculations a supercell of a few hundreds atoms is simulated by quantum molecular dynamics method using usually approximation with only one k-point. Periodical boundary conditions are hold on the walls of a supercell. Simulations starts from a configuration with atoms in lattice. Gradually during ionic displacements the ionic temperature increases up to a predetermined value. After that temperature T_i becomes fixed. A set of ionic configurations are accumulated during motion of atoms in supercell along a trajectory of many-body system. After that every particular configuration in this set is used for DFT calculation of conductivities. Results for every configuration are averaged around the set. Calculations of conductivities are based on Kubo-Greenwood relation. Those calculations are more difficult in case of solid.

Comparisons of our results are shown in Fig. 8 (middle) for Au and in Fig. 8 (right) for aluminum. MD DFT/Kubo-Greenwood results presented in Fig. 8 (middle) are obtained for system containing 32 atoms.[18] A mesh with $2 * 2 * 2$ k-points is used. Density of gold is taken equal 19.32 g/cm^3. DFT results for solid gold $T_i = 0.3$ kK better agree with our calculations at elevated temperatures T_e. At smaller values T_e disagreement is larger. DFT does not follow the local maximum of thermal conductivity.

In Fig. 8 (right) comparison in case of of aluminum is shown. Two examples are presented; density is 2.7 g cm^{-3} for both examples. First of them corresponds to a one-temperature case: $T = T_e = T_i$. While another refers to a 2T case with fixed temperature $T_i = 3$ kK. Both examples are taken from paper.[19] We see that our results satisfactory agree with DFT in wide range of temperatures.

6. CONTRIBUTIONS TO ELECTRICAL AND THERMAL CONDUCTIVITIES DUE TO ELECTRON-PHONON INTERACTION IN TWO-TEMPERATURE STATE WITH ELEVATED ELECTRON TEMPERATURES

When considering the electron heat transfer coefficient κ, we must take into account the growth of electron-electron interaction contribution in addition to the electron-ion scattering at high electron temperatures here

considered. Now we consider how electron-phonon interaction contributes into the electron heat transfer coefficient at high electron temperatures.

We consider metals with s-, p- and d-electron energy bands excited by the laser irradiation. Electron spectra in our approach is approximated by the parabolic expressions, different for s-, p-electrons (which we call simply s-electrons) and d-electrons: $\varepsilon(\mathbf{p}) = \varepsilon_s + p^2/2m_s$, if $\mathbf{p} \in s$ and $\varepsilon(\mathbf{p}') = \varepsilon_1 + p'^2/2m_d$, if $\mathbf{p}' \in d$. Electrons in these bands have effective masses m_s and m_d respectively. Parameters of the parabolic approach are chosen in order to approximate the density of state calculations by the density functional method (DFT, see Section 2 above). Short version of our approach has been presented in paper.[7] It does not include description of important geometrical restrictions imposed on our integrals. Electron energy in s-band lies in the interval $\varepsilon_s \leq \varepsilon$, while in d-band it is restricted by the finite interval $\varepsilon_1 \leq \varepsilon \leq \varepsilon_2$. Electron s- and d-band Fermi functions have the form $f_s(\mathbf{p}) = [1 + e^{(\varepsilon(\mathbf{p})-\mu)/k_B T_e}]^{-1}$, if $\mathbf{p} \in s$ and $f_d(\mathbf{p}') = [1 + e^{(\varepsilon(\mathbf{p}')-\mu)/k_B T_e}]^{-1}$, if $\mathbf{p}' \in d$ with common chemical potential $\mu(T_e)$ and temperature T_e. Phonon distribution function at ion temperature T_i has the form $N(\mathbf{q}) = [e^{\hbar\omega_{\mathbf{q}}/k_B T_i} - 1]^{-1}$. Dependence of the phonon frequency ω on its quasimomentum $\mathbf{q}$ is chosen to be $\omega(q) = sq(1 - q/q_D(2 - 3\zeta) + (q/q_D)^2(1 - 2\zeta))$ with q_D being the Debye momentum and ζ is responsible for the deviation of spectra of acoustical phonons from linear form at large values of momenta.

6.1 s- and d-electron Scattering within the Relaxation Time Approach

The number of s-electrons escaping from the 3D element $d\mathbf{p}$ in unit time, can be written as[27]

$$\dot{N}^s_- = \dot{N}^{s,s+ph}_- + \dot{N}^{s,d+ph}_- + \dot{N}^{s+ph,s}_- + \dot{N}^{s+ph,d}_-,$$

where

$$\dot{N}^{s,s+ph}_- = f_s(\mathbf{p}) \frac{2d\mathbf{p}}{(2\pi\hbar)^3} \int W^{ss}(q)\delta(\varepsilon - \varepsilon')(1 - f_s(\mathbf{p}'))(N_{\mathbf{q}} + 1)\frac{Vd\mathbf{p}'}{(2\pi\hbar)^3} \tag{7}$$

is the number of s-electrons with the energy ε escaping from the $d\mathbf{p}$ element per unit volume into another states $\mathbf{p}'$ within the same s-band with the energy ε' because of the emission of phonons ($\mathbf{p} \to \mathbf{p}' + \mathbf{q}$ process), V is a system volume. The rate

$$\dot{N}^{s,d+ph}_- = f_s(\mathbf{p}) \frac{2d\mathbf{p}}{(2\pi\hbar)^3} \int W^{sd}(q)\delta(\varepsilon - \varepsilon')(1 - f_s(\mathbf{p}'))N_{\mathbf{q}}\frac{Vd\mathbf{p}'}{(2\pi\hbar)^3} \tag{8}$$

describes the number of s-electrons escaping from the $d\mathbf{p}$ element into states in d-band because of the phonon emission. Correspondingly $\dot{N}^{s+ph,s}_-$ and $\dot{N}^{s+ph,d}_-$ denote numbers of s-electrons escaping from the $d\mathbf{p}$ element into states in s- and d-bands because of the absorption of phonons ($\mathbf{p}' \to \mathbf{p} + \mathbf{q}$ process). Delta-function in (7) and (8) describes electron energy conservation and doesn't include negligibly small phonon energy.

By the similar way we can write the number of s-electrons, incoming to the element $d\mathbf{p}$ in unit time

$$\dot{N}^s_+ = \dot{N}^{s,s+ph}_+ + \dot{N}^{s,d+ph}_+ + \dot{N}^{s+ph,s}_+ + \dot{N}^{s+ph,d}_+$$

with

$$\dot{N}^{s,s+ph}_+ = (1 - f_s(\mathbf{p})) \frac{2d\mathbf{p}}{(2\pi\hbar)^3} \int W^{ss}(q)\delta(\varepsilon - \varepsilon')(1 - f_s(\mathbf{p}'))(N_{\mathbf{q}} + 1)\frac{Vd\mathbf{p}'}{(2\pi\hbar)^3} \tag{9}$$

and

$$\dot{N}^{s,d+ph}_+ = (1 - f_s(\mathbf{p})) \frac{2d\mathbf{p}}{(2\pi\hbar)^3} \int W^{sd}(q)\delta(\varepsilon - \varepsilon')(1 - f_s(\mathbf{p}'))(N_{\mathbf{q}} + 1)\frac{Vd\mathbf{p}'}{(2\pi\hbar)^3} \tag{10}$$

standing for the number of s-electrons, incoming to the element $d\mathbf{p}$ from s- and d- bands correspondingly because of the emission of phonons. The terms $\dot{N}^{s+ph,s}_+$ and $\dot{N}^{s+ph,d}_+$ give the number of s-electrons incoming to the $d\mathbf{p}$ element from s- and d-bands accordingly because of phonon absorption. Resulting rate of change of the number of s-electrons in unit phase volume as a result of electron-phonon collisions is

$$\dot{N}_s(\mathbf{p}) = \dot{N}^s_+ - \dot{N}^s_- = \int_{\mathbf{p}' \in s} W^{ss}(q) \cdot \delta(\varepsilon - \varepsilon') \cdot [f_s(\mathbf{p}') - f_s(\mathbf{p})] \cdot (2N_{\mathbf{q}} + 1)\frac{Vd\mathbf{p}'}{(2\pi\hbar)^3} +$$

$$+\int_{\mathbf{p}'\in d} W^{sd}(q)\cdot\delta(\varepsilon-\varepsilon')\cdot[f_d(\mathbf{p}')-f_s(\mathbf{p})]\cdot(2N_{\mathbf{q}}+1)\frac{Vd\mathbf{p}'}{(2\pi\hbar)^3}.$$

On the other hand the rate of change of the number of s-electrons in unit phase volume is df_s/dt, so the kinetic equation is obtained by the ordinary way

$$\frac{df_s}{dt}=\frac{\partial f_s}{\partial\mathbf{p}}\cdot e\mathbf{E}=(f_s)'_\varepsilon\frac{\mathbf{p}}{m_s}\cdot e\mathbf{E}=\dot{N}_s,$$

where m_s is the effective mass of s-electrons and $(f_s)'_\varepsilon=\partial f_s/\partial\varepsilon$. By the similar way we obtain the rate of change of the number of d-electrons in unit phase volume owing to the electron-phonon collisions

$$\dot{N}_d(\mathbf{p}')=\int_{\mathbf{p}\in d} W^{dd}(q)\cdot\delta(\varepsilon-\varepsilon')\cdot[f_d(\mathbf{p})-f_d(\mathbf{p}')]\cdot(2N_{\mathbf{q}}+1)\frac{Vd\mathbf{p}}{(2\pi\hbar)^3}+$$

$$+\int_{\mathbf{p}\in s} W^{ds}(q)\cdot\delta(\varepsilon-\varepsilon')\cdot[f_s(\mathbf{p})-f_d(\mathbf{p}')]\cdot(2N_{\mathbf{q}}+1)\frac{Vd\mathbf{p}}{(2\pi\hbar)^3}$$

and the kinetic equation for d-electrons

$$\frac{df_d}{dt}=\frac{\partial f_d}{\partial\mathbf{p}'}\cdot e\mathbf{E}=(f_d)'_\varepsilon\frac{\mathbf{p}'}{m_d}\cdot e\mathbf{E}=\dot{N}_d,$$

Within the relaxation time approximation we have

$$df/dt=-(f-f_0)/\tau(\mathbf{p})=-f_1(\mathbf{p})/\tau(\mathbf{p})=(e/m^*)f'_\varepsilon\,\mathbf{pE}.$$

Here we have $f=f_0+f_1$, where f_0 is the equilibrium distribution function in the absence of electric field and $f_1=(e/m^*)(-f'_\varepsilon)\,\mathbf{pE}\,\tau(\mathbf{p})$ is correction to it.

We introduce small corrections to the equilibrium distribution functions of s- and d-electrons

$$f_1^s(\mathbf{p})=\eta_s(\varepsilon)\mathbf{pE}\tau_s(\varepsilon),\qquad f_1^d(\mathbf{p}')=\eta_d(\varepsilon)\mathbf{p}'\mathbf{E}\tau_d(\varepsilon).$$

Then linearization of kinetic equations gives for s-electrons

$$-\eta_s(\varepsilon)\mathbf{pE}=\int_{\mathbf{p}'\in s} W^{ss}(q)\delta(\varepsilon-\varepsilon')\left[\eta_s(\varepsilon)\mathbf{p}'\mathbf{E}\tau_s(\varepsilon)-\eta_s(\varepsilon)\mathbf{pE}\tau_s(\varepsilon)\right](2N_{\mathbf{q}}+1)\frac{Vd\mathbf{p}'}{(2\pi\hbar)^3}+$$

$$+\int_{\mathbf{p}'\in d} W^{sd}(q)\delta(\varepsilon-\varepsilon')\left[\eta_d(\varepsilon)\mathbf{p}'\mathbf{E}\tau_d(\varepsilon)-\eta_s(\varepsilon)\mathbf{pE}\tau_s(\varepsilon)\right](2N_{\mathbf{q}}+1)\frac{Vd\mathbf{p}'}{(2\pi\hbar)^3}$$

But we have

$$\mathbf{p}'\mathbf{E}=p'E\cos\alpha'=p'E(\cos\alpha\cos\theta+\sin\alpha\sin\theta\cos\phi),$$

where α is the angle between vectors $\mathbf{p}$ and $\mathbf{E}$, α' is the angle between vectors $\mathbf{p}'$ and $\mathbf{E}$, θ is the angle between vectors $\mathbf{p}$ and $\mathbf{p}'$. After the integration over the angle ϕ between the planes $(\mathbf{pp}')$ and $(\mathbf{pE})$ we obtain

$$\mathbf{p}'\mathbf{E}=p'E\cos\alpha\cos\theta=\frac{p}{p}pE\cos\alpha\cos\theta=\frac{p'}{p}\mathbf{pE}\cos\theta.$$

Because of the energy conservation at s-s collisions we have $p'=p$. Taking into account that $q^2=p^2+p'^2+2pp't$, $dt=qdq/(pp')$, and $d\mathbf{p}'=2\pi p'^2dp'dt=2\pi\,p'qdp'dq/p=2\pi m^*qd\varepsilon'dq/p$, we have for s-electrons after canceling the common factor $\mathbf{pE}$

$$-\eta_s(\varepsilon)=\int_{\mathbf{p}'\in s} W^{ss}(q)\delta(\varepsilon-\varepsilon')\left[\eta_s(\varepsilon)cos\theta\tau_s(\varepsilon)-\eta_s(\varepsilon)\tau_s(\varepsilon)\right](2N_{\mathbf{q}}+1)\frac{V}{(2\pi\hbar)^3}\frac{2\pi m_s}{p}qd\varepsilon'dq+$$

$$+\int_{\mathbf{p}'\in d} W^{sd}(q)\delta(\varepsilon-\varepsilon')\left[\eta_d(\varepsilon)\frac{p'}{p}\cos\theta\tau_d(\varepsilon)-\eta_s(\varepsilon)\tau_s(\varepsilon)\right](2N_{\mathbf{q}}+1)\frac{V}{(2\pi\hbar)^3}\frac{2\pi m_d}{p}qd\varepsilon' dq.$$

Integration over ε' with taking into account δ-function gives

$$-\eta_s(\varepsilon)=\eta_s(\varepsilon)\tau_s(\varepsilon)\int_s W^{ss}(q)(\cos\theta-1)(2N_{\mathbf{q}}+1)\frac{V}{(2\pi\hbar)^3}\frac{2\pi m_s}{p}qdq+$$

$$+\eta_d(\varepsilon)\tau_d(\varepsilon)\int_d W^{sd}(q)\frac{p'}{p}\cos\theta(2N_{\mathbf{q}}+1)\frac{V}{(2\pi\hbar)^3}\frac{2\pi m_d}{p}qdq-\eta_s(\varepsilon)\tau_s(\varepsilon)\int_d W^{sd}(q)(2N_{\mathbf{q}}+1)\frac{V}{(2\pi\hbar)^3}\frac{2\pi m_d}{p}qdq.$$

We denote

$$\int_s W^{ss}(q)(1-\cos\theta)(2N_{\mathbf{q}}+1)\frac{V}{(2\pi\hbar)^3}\frac{2\pi m_s}{p}qdq=H_{ss}(\varepsilon),$$

$$\int_d W^{sd}(q)\frac{p\prime}{p}\cos\theta(2N_{\mathbf{q}}+1)\frac{V}{(2\pi\hbar)^3}\frac{2\pi m_d}{p}qdq=H_{sd}(\varepsilon),$$

$$\int_d W^{sd}(q)(2N_{\mathbf{q}}+1)\frac{V}{(2\pi\hbar)^3}\frac{2\pi m_d}{p}qdq=G_{sd}(\varepsilon).$$

Then the kinetic equation for s-electrons takes the form

$$\eta_s(H_{ss}+G_{sd})\tau_s-\eta_d H_{sd}\tau_d=\eta_s. \tag{11}$$

Analogously for d-electrons it can be obtained

$$-\eta_d(\varepsilon)=\eta_d(\varepsilon)\tau_d(\varepsilon)\int_d W^{dd}(q)(\cos\theta-1)(2N_{\mathbf{q}}+1)\frac{V}{(2\pi\hbar)^3}\frac{2\pi m_d}{p'}qdq+$$

$$+\eta_s(\varepsilon)\tau_s(\varepsilon)\int_s W^{ds}(q)\frac{p}{p}\cos\theta(2N_{\mathbf{q}}+1)\frac{V}{(2\pi\hbar)^3}\frac{2\pi m_s}{p'}qdq-\eta_d(\varepsilon)\tau_d(\varepsilon)\int_s W^{ds}(q)(2N_{\mathbf{q}}+1)\frac{V}{(2\pi\hbar)^3}\frac{2\pi m_s}{p'}qdq$$

Denoting

$$\int_d W^{dd}(q)(1-\cos\theta)(2N_{\mathbf{q}}+1)\frac{V}{(2\pi\hbar)^3}\frac{2\pi m_d}{p'}qdq=H_{dd}(\varepsilon),$$

$$\int_s W^{ds}(q)\frac{p}{p}\cos\theta(2N_{\mathbf{q}}+1)\frac{V}{(2\pi\hbar)^3}\frac{2\pi m_s}{p'}qdq=H_{ds}(\varepsilon),$$

$$\int_s W^{ds}(q)(2N_{\mathbf{q}}+1)\frac{V}{(2\pi\hbar)^3}\frac{2\pi m_s}{p'}qdq=G_{ds}(\varepsilon)$$

we introduce the second equation for τ_s and τ_d:

$$\eta_s H_{ds}\tau_s-\eta_d(H_{dd}+G_{ds})\tau_d=-\eta_d. \tag{12}$$

From the system of equations (11) and (12) in the case when transition between s- and d- bands exists we find

$$\tau_s(\varepsilon)=\frac{\frac{\eta_d}{\eta_s}H_{sd}+H_{dd}+G_{ds}}{(H_{ss}+G_{sd})(H_{dd}+G_{ds})-H_{sd}H_{ds}},$$

$$\tau_d(\varepsilon)=\frac{\frac{\eta_s}{\eta_d}H_{ds}+H_{ss}+G_{sd}}{(H_{ss}+G_{sd})(H_{dd}+G_{ds})-H_{sd}H_{ds}}.$$

Taking into account that $\eta_s/\eta_d=m_d/m_s$, we have

$$\tau_s(\varepsilon)=\frac{\frac{m_s}{m_d}H_{sd}+H_{dd}+G_{ds}}{(H_{ss}+G_{sd})(H_{dd}+G_{ds})-H_{sd}H_{ds}},$$

$$\tau_d(\varepsilon)=\frac{\frac{m_d}{m_s}H_{ds}+H_{ss}+G_{sd}}{(H_{ss}+G_{sd})(H_{dd}+G_{ds})-H_{sd}H_{ds}}.$$

In the case when s- electron has a momentum allowing only $s\to s$ scattering, we have simply $\tau_s(\varepsilon)=1/H_{ss}$.

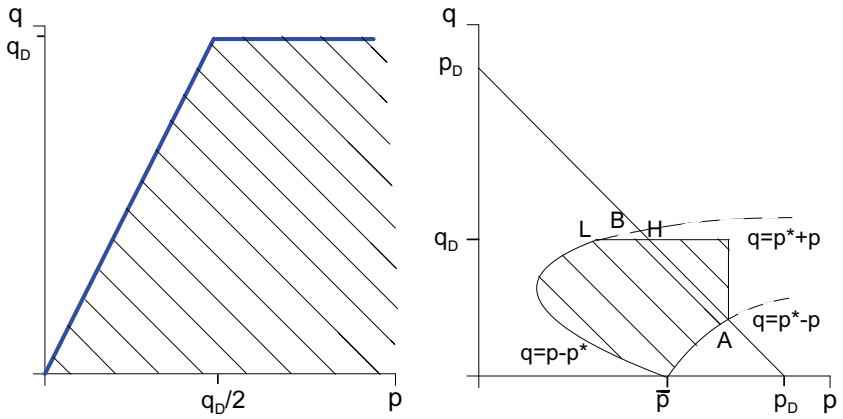

Figure 9. The range of integration over q and p when calculating the contribution of $s \to s$ and $s \to d$ scatterings into electrical conductivity and electron heat conductivity due to electron-phonon interaction. *Left panel.* Region in $q-p$-plane for the integration when calculating the contribution of $s \to s$ processes into the electron transport coefficients owing to the electron-phonon interaction. *Right panel.* (q-p)-region of integration for $s \to d$-process.

6.2 Regions of Integration in (q-p)-plane in Matrix Elements H and G

When calculating relaxation times τ_s and τ_d, integration over ε', deleting δ-function, is made. To make it possible with the nonzero result, restrictions on the range of integration in (p,q)-plane arise.

When considering $s \to s$-scattering, we have: $\mathbf{p}+\mathbf{q}=\mathbf{p}'$, $q^2 = p^2 + p'^2 - 2\mathbf{p}\mathbf{p}'$. Here $\mathbf{p}$ stands for the s-electron momentum before the collision, $\mathbf{p}'$ is the s-electron momentum after the collision. We introduce the angle θ between vectors $\mathbf{p}$ and $\mathbf{p}'$ and also the variable $t' = -cos\theta$. Then $q^2 = p^2 + p'^2 + 2pp't'$ and $dt' = qdq/(pp')$. Volume element in $\mathbf{p}'$-space is equal to

$$d\mathbf{p}' = 2\pi p'^2 dp' \frac{qdq}{pp'} = 2\pi \frac{q}{p} p' dp' dq = 2\pi \frac{q}{p} m_s d\varepsilon' dq$$

($\varepsilon' = \varepsilon_s + p'^2/(2m_s)$ is the energy of s-electron after the collision). At given q the momentum p' has values from $p'_{min} = |p-q|$ to $p'_{max} = p+q$. Presence of function $\delta(\varepsilon' - \varepsilon)$ leads to conditions

$$\varepsilon_s + \frac{(p-q)^2}{2m_s} < \varepsilon_s + \frac{p^2}{2m_s}, \qquad \varepsilon_s + \frac{(p+q)^2}{2m_s} > \varepsilon_s + \frac{p^2}{2m_s}.$$

First of these inequalities gives $q < 2p$. Together with the restriction $q < q_D$ it defines the range of integration in (q,p)-plane, shown in Fig. 9 (left) by the hatched region.

Let's consider $s \to d$ scattering: $\mathbf{p}+\mathbf{q}=\mathbf{p}'$, $q^2 = p^2 + p'^2 - 2\mathbf{p}\mathbf{p}'$. Here $\mathbf{p}$ is the momentum of s-electron, $\mathbf{p}'$ is the momentum of d-electron. Now we introduce the angle θ between vectors $\mathbf{p}$ and $\mathbf{p}'$ as well as a variable $t' = -cos\theta$. Then $q^2 = p^2 + p'^2 + 2pp't'$ and $dt' = qdq/(pp')$, so volume element in $\mathbf{p}'$-space can be written as

$$d\mathbf{p}' = 2\pi p'^2 dp' \frac{qdq}{pp'} = 2\pi \frac{q}{p} p' dp' dq = 2\pi \frac{q}{p} m_d d\varepsilon' dq.$$

Here $\varepsilon' = \varepsilon_1 + p'^2/(2m_d)$ is the energy of d-electron. We introduce the boundary momentum of the electron in d-band $p_d = \sqrt{2m_d(\varepsilon_2 - \varepsilon_1)}$. At given q the value p' lies from $p'_{min} = |p-q|$ to $p'_{max} = p+q$. In dependence on positions of values p'_{min}, p'_{max}, p_d different situations are possible.

Case sd-1. $|p-q| < p+q < p_d$

Energy of s-electron is $\varepsilon = \varepsilon_s + p^2/(2m_s)$. Function $\delta(\varepsilon' - \varepsilon)$ at given positions of characteristic points in addition to inequality $p+q < p_d$ creates restrictions in the form of inequalities

$$\varepsilon_1 + \frac{(p-q)^2}{2m_d} < \varepsilon_s + \frac{p^2}{2m_s}, \qquad \varepsilon_1 + \frac{(p+q)^2}{2m_d} > \varepsilon_s + \frac{p^2}{2m_s}.$$

A system of these three inequalities can be written as

$$(p-q)^2 < 2m_d(\varepsilon-\varepsilon_1), \qquad (p+q)^2 > 2m_d(\varepsilon-\varepsilon_1), \qquad p+q < p_d.$$

When denoting $p_*(\varepsilon) = \sqrt{2m_d(\varepsilon-\varepsilon_1)}$ and adding to three inequalities above the restriction on phonon quasi-momentum $q < q_D$, we obtain a system of inequalities

$$p - p_* < q < p + p_*, \qquad q > p_* - p, \qquad q < p_d - p, \qquad q < q_D.$$

Region of (q, p) variables, described by these inequalities, is shown in Fig. 9 (right) by the hatched region below the line $q = p_d - p$.

We introduce notations $m_0 = \sqrt{m_d/m_s}$ and $p_{1s} = \sqrt{2m_s(\varepsilon_1-\varepsilon_s)}$, $p_{2s} = \sqrt{2m_s(\varepsilon_2-\varepsilon_s)}$. And we also introduce a value of momentum of s-electron $\bar{p}$, at which $p_* - p = 0$. We can find $\bar{p} = \sqrt{2\bar{m}(\varepsilon_1-\varepsilon_s)}$, where $1/\bar{m} = 1/m_s - 1/m_d$.

Points A, B, H, L shown in Fig. 9 (right) have p-coordinates: $p(A) = p_{2s}$, $p(B) = (\sqrt{4\,p_d^2 + m_0^2(m_0^2-4)p_{2s}^2} - 2p_d)/(m_0^2-4)$, $p(H) = p_d - q_D$, $p(L) = (m_0\sqrt{q_d^2 + (m_0^2-1)p_{1s}^2} - q_D)/(m_0^2-1)$.

Analogously the range of integration in (q, p)-plane can be obtained in the case corresponding to the alternative case of relative positions of values p'_{min}, p'_{max}, and p_d.

Case sd-2. $|p-q| < p_d < p+q$

It gives equivalently

$$p - p_d < q < p + p_d, \qquad q > p_d - p.$$

Because of energy δ-function the following two restrictions

$$\varepsilon_1 + \frac{(p-q)^2}{2m_d} < \varepsilon_s + \frac{p^2}{2m_s}, \qquad \varepsilon_1 + \frac{p_d^2}{2m_d} > \varepsilon_s + \frac{p^2}{2m_s}.$$

arise. With the use of introduced designations they can be written as $(p-q)^2 < p_*^2$, $p < p_{2s}$. As a result a system of inequalities

$$p - p_d < q < p + p_d, \qquad q > p_d - p, \qquad p - p_* < q < p + p_*, \qquad p < p_{2s}, \qquad q < q_D$$

is obtained. The range defined by these inequalities (having triangular form) is also shown in Fig. 9 (right) by the hatched region above the line $q = p_d - p$.

Now we consider $d \to s$ scattering. Electron in d-band having the momentum $\mathbf{p}'$ is scattered to s-band to obtain the momentum $\mathbf{p}$ with the transferred momentum $\mathbf{q} = \mathbf{p}' - \mathbf{p}$. By introducing the angle θ between $\mathbf{p}'$ and $\mathbf{p}$ and designation $t' = -\cos\theta$, we have $q^2 = p^2 + p'^2 + 2p\,p'\,t'$, $dt' = qdq/(pp')$. Now the integration over the final states is the integration over the states $\mathbf{p}$ of s-electron. The volume element in $\mathbf{p}$-space of final states of electron after the scattering can be written as

$$d\mathbf{p} = 2\pi\,p^2\,dp\,dt' = 2\pi\,p^2\,dp\,\frac{qdq}{pp'} = 2\pi\frac{pq}{p'}dp\,dq = 2\pi\frac{q}{p'}m_s\,d\varepsilon\,dq.$$

At a given q the s-electron momentum changes from $p_{min} = |p'-q|$ up to $p_{max} = p'+q$. In addition to the inequality $p' < p_d$, because of the presence of δ-function, a system of inequalities

$$\varepsilon_s + \frac{(p'-q)^2}{2m_s} < \varepsilon', \qquad \varepsilon_s + \frac{(p'+q)^2}{2m_s} > \varepsilon'$$

or

$$(p'-q)^2 < 2m_s(\varepsilon-\varepsilon_s), \qquad (p'+q)^2 > 2m_s(\varepsilon-\varepsilon_s), \qquad p' < p_d$$

arises. We denote $p_*(\varepsilon') = \sqrt{2m_s(\varepsilon'-\varepsilon_s)}$. Then the system of these inequalities can be written as

$$p' - p'_* < q < p' + p'_*, \qquad q > p'_* - p', \qquad p' < p_d, \qquad q < q_D.$$

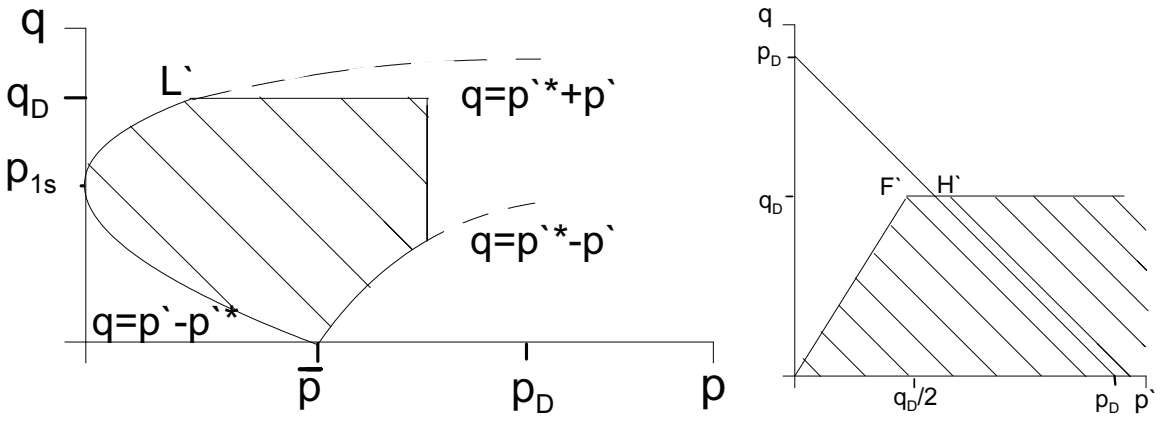

Figure 10. The range of the $q-p'$-plane for the integration of electron transport coefficients because of electron $d\to s$ and $d\to d$ transitions after the electron-phonon interaction. *Left panel.* Region for integration in the plane of q and p' variables to obtain electrical conductivity and electron heat conductivity due to the electron-phonon interaction when $d\to s$ scattering takes place. *Right panel.* Part of $q-p'$-plane for the integration designed to calculate $d\to d$-contribution.

The range of variables (q,p'), defined by the system of these inequalities, is presented in Fig. 10 (left). Point L$'$ in Fig. 10 (left) has the coordinate $p'\,(\mathrm{L}')=m_0\,(m_0q_D-\sqrt{q_D^2+(m_0^2-1)p_{1s}^2})/(m_0^2-1)$.

It only remains to consider $d\to d$ scattering. d-electron with the momentum $\mathbf{p}'$ is scattered to d-band, taking on the momentum $\mathbf{p}''$ with the transferred value of momentum $\mathbf{q}=\mathbf{p}'-\mathbf{p}''$. When introducing the angle θ between vectors $\mathbf{p}'$ and $\mathbf{p}''$ and designation $t=-\cos\theta$, we obtain $q^2=p''^2+p'^2+2\,p''\,p'\,t,\ \ dt=q\,dq/p''\,p'$. Now the integration over final states implies the integration over the states of d-electron $\mathbf{p}''$. We have

$$d\mathbf{p}''=2\pi\,p''^2\,dp''\,dt=2\pi\frac{p''\,q}{p'}dp''\,dq=2\pi\frac{q}{p'}m_d\,d\varepsilon''\,dq.$$

At a given q the momentum of scattered electron in d-band is changed from $p''_{min}=|p-q|$ to $p''_{max}=p+q$. In dependence on interpositions of p''_{min}, p''_{max}, p_d two cases can be considered:

Case dd-1. $\quad |p'-q|<p'+q<p_d$

δ-function leads to the system of inequalities, additional to the condition $p'<p_d$:

$$\varepsilon_1+\frac{(p'-q)^2}{2m_d}<\varepsilon_1+\frac{p'^2}{2m_d},\qquad \varepsilon_1+\frac{(p'+q)^2}{2m_d}>\varepsilon_1+\frac{p'^2}{2m_d},$$

whence it follows that

$$(q-p')^2<p'^2,\qquad (q+p')^2>p'^2.$$

As a result a system of inequalities arises:

$$q<2p',\qquad q<p_d-p',\qquad p'<p_d,\qquad q<q_D.$$

The range in (q,p')-plane, restricted by these inequalities, is shown in Fig. 10 (right) under the line $q=p_d-p'$. Characteristic points here have p'-coordinates: $p'(F')=q_D/2,\ \ p'(H')=p_d-q_D$.

Case dd-2. $\quad |p'-q|<p_d<p'+q$

Now we add to the inequality $|p'-q|<p_d<p'+q$ the inequalities arising due to the presence of δ-function:

$$\varepsilon_1+\frac{(p'-q)^2}{2m_d}<\varepsilon_1+\frac{p'^2}{2m_d},\qquad \varepsilon_1+\frac{p_d^2}{2m_d}>\varepsilon_1+\frac{p'^2}{2m_d}.$$

Resulting system of inequalities has the form

$$q < 2p', \qquad q > p_d - p', \qquad p' < p_d, \qquad q < q_D, \qquad p' - p_d < q < p' + p_d.$$

Corresponding range of (q, p') variables is also shown in Fig. 10 (right) as a triangle over the line $q = p_d - p'$. Now let's consider matrix elements H and G. Taking into account that when $s \to s$-scattering, the angle between initial and scattered electrons θ satisfies the relation $\cos\theta = 1 - q^2/(2p^2),$, when $s \to d$ and $d \to s$-scattering, $\cos\theta = (p^2 + p'^2 - q^2)/(2pp')$, and finally, when $d \to d$-scattering, $\cos\theta = 1 - q^2/(2p'^2)$, we can write these matrix elements in the form

$$H_{ss}(\varepsilon) = \int Z_{ss}^2 W(q) \frac{q^2}{2p^2}(2N_{\mathbf{q}} + 1)\frac{V}{(2\pi\hbar)^3}\frac{2\pi m_s}{p} qdq,$$

$$H_{sd}(\varepsilon) = \int Z_{sd}^2 W(q) \frac{p'}{p}\frac{p^2 + p'^2 - q^2}{2pp'}(2N_{\mathbf{q}} + 1)\frac{V}{(2\pi\hbar)^3}\frac{2\pi m_d}{p} qdq,$$

$$G_{sd}(\varepsilon) = \int Z_{sd}^2 W(q)(2N_{\mathbf{q}} + 1)\frac{V}{(2\pi\hbar)^3}\frac{2\pi m_d}{p} qdq,$$

$$H_{dd}(\varepsilon) = \int Z_{dd}^2 W(q) \frac{q^2}{2p'^2}(2N_{\mathbf{q}} + 1)\frac{V}{(2\pi\hbar)^3}\frac{2\pi m_d}{p'} qdq,$$

$$H_{ds}(\varepsilon) = \int Z_{ds}^2 W(q) \frac{p}{p'}\frac{p^2 + p'^2 - q^2}{2pp'}(2N_{\mathbf{q}} + 1)\frac{V}{(2\pi\hbar)^3}\frac{2\pi m_s}{p} qdq,$$

$$G_{ds}(\varepsilon) = \int Z_{ds}^2 W(q)(2N_{\mathbf{q}} + 1)\frac{V}{(2\pi\hbar)^3}\frac{2\pi m_s}{p'} qdq. \tag{13}$$

Here we have introduced a function

$$W(q) = \frac{\pi q^2}{\rho V \omega}\left(\frac{4\pi n e^2\hbar^2}{q^2\epsilon(q)}\right)^2$$

with $n, \rho, \epsilon(q)$ being correspondingly concentration of atoms, their mass density, and electron dielectric permittivity to write for example W^{ss} as $W^{ss} = Z_{ss}^2 W(q)$ and analogously write another transition probabilities. $Z_{ss}, Z_{sd}, Z_{ds}, Z_{dd}$ are effective charges for corresponding scattering process. Matrix elements H and G are defined by the energy of electron, which is held constant after the scattering because of the quasielastic character of electron-phonon interaction. So that if the change between s- and d-bands takes place, we have

$$\varepsilon = \varepsilon_s + \frac{p^2}{2m_s} = \varepsilon_1 + \frac{p'^2}{2m_d}$$

In this case the momentum of electron in d-band p is a single-valued function of the momentum p of electron in s-band. We shall use the momentum of electron in s-band. When we use designations introduced by

$$p' = m_0\sqrt{p^2 - p_{1s}^2}, \tag{14}$$

and it exists only at $p \geq p_{1s}$. For smaller values of momentum the s-electron can be scattered only to s-band. Electron transfer from s- no d-band begins only when s-electron momentum satisfies inequality $p \geq p_{1s}$. As a result, when taking the momentum of s- electron as a parameter, we obtain for different intervals of p the following limits of integration over q on calculating the matrix elements H and G:

$1)0 < p < \frac{q_D}{2}$

$\int_0^{2p} dq[ss]$

$2)\frac{q_D}{2} < p < p_{1s}$

$\int_0^{q_D} dq[ss]$

$3) p_{1s} < p < p_L \qquad (p_L = p(p'(L'))$

$\int_0^{q_D} dq[ss] + \int_{p-p_*}^{p+p_*} dq[sd] + \int_{p'_*-p'}^{p'+p'_*} dq[ds] + \int_0^{2p'} dq[dd]$

$4) p_L < p < p(p'(F'))$

$\int_0^{q_D} dq[ss] + \int_{p-p_*}^{q_D} dq[sd] + \int_{p'_*-p'}^{q_D} dq[ds] + \int_0^{2p'} dq[dd]$

$5) p(p'(F')) < p < \bar{p}$

$\int_0^{q_D} dq[ss] + \int_{p-p_*}^{q_D} dq[sd] + \int_{p'_*-p'}^{q_D} dq[ds] + \int_0^{q_D} dq[dd]$

$6) \bar{p} < p < p_{2s}$

$\int_0^{q_D} dq[ss] + \int_{p_*-p}^{q_D} dq[sd] + \int_{p'-p'_*}^{q_D} dq[ds] + \int_0^{q_D} dq[dd]$

$7) p > p_{2s}$

$\int_0^{q_D} dq[ss]$

Here symbols $[ss], [sd], [ds], [dd]$ stand for the type of a scattering for the matrix elements H and G, which defines their value in accordance with equations (13).

6.3 Electrical Conductivity and Electron Heat Conductivity Owing to Interaction of s- and d-electrons with Phonons

Relaxation times obtained as functions of electron momentum being substituted into the expressions for the electrical conductivity of s- and d-electrons, deduced from kinetic equations within the relaxation time approach, give a resistivity and effective frequencies of electron-phonon collisions in dependence of electron temperature.

Current density in the electric field direction being in line with the z-axis, can be written as

$$j_z = e \int f_1(p) v_z 2 \frac{d^3p}{(2\pi\hbar)^3} = e^2 \int \left(-\frac{\partial f_0}{\partial \varepsilon}\right) \mathbf{vE} \tau(p) v_z \frac{d^3p}{(2\pi\hbar)^3} =$$

$$= e^2 \int \left(-\frac{\partial f_0}{\partial \varepsilon}\right) \tau(p) v_z^2 2 \frac{d^3p}{(2\pi\hbar)^3} E_z = e^2 \int_p \int_0^{\pi} \left(-\frac{\partial f_0}{\partial \varepsilon}\right) \frac{p^2}{m^{*2}} \cos^2\theta \, \tau(p) \, 2 \, \frac{2\pi \, p^2 \, dp \, d(-\cos\theta)}{(2\pi\hbar)^3} E_z.$$

Thus electrical conductivity is equal to

$$\sigma = \frac{2}{3} \left(\frac{e}{m^*}\right)^2 \frac{4\pi}{(2\pi\hbar)^3} \int_p \left(-\frac{\partial f_0}{\partial \varepsilon}\right) \tau(p) \frac{p^4 dp}{(2\pi\hbar)^3}$$

Electrical conductivity due to the s-electrons then equals to

$$\sigma_s = \frac{2}{3} \left(\frac{e}{m_s}\right)^2 \frac{4\pi}{(2\pi\hbar)^3} \int_p \left(-\frac{\partial f_{0s}}{\partial \varepsilon}\right) \tau_s(p) \frac{p^4 dp}{(2\pi\hbar)^3}, \quad \text{with} \quad -\frac{\partial f_{0s}}{\partial \varepsilon} = \frac{\exp[(\varepsilon-\mu)/kT_e]/kT_e}{\exp[(\varepsilon-\mu)/kT_e]+1} \quad \text{and} \quad \varepsilon = \varepsilon_s + \frac{p^2}{2m_s}.$$

Accordingly electrical conductivity through d-electrons can be written as

$$\sigma_d = \frac{2}{3} \left(\frac{e}{m_d}\right)^2 \frac{4\pi}{(2\pi\hbar)^3} \int_p' \left(-\frac{\partial f_{0d}}{\partial \varepsilon'}\right) \tau_d(p') \frac{p'^4 dp'}{(2\pi\hbar)^3}, \quad \text{where} \quad -\frac{\partial f_{0d}}{\partial \varepsilon'} = \frac{\exp[(\varepsilon'-\mu)/kT_e]/kT_e}{\exp[(\varepsilon'-\mu)/kT_e]+1}.$$

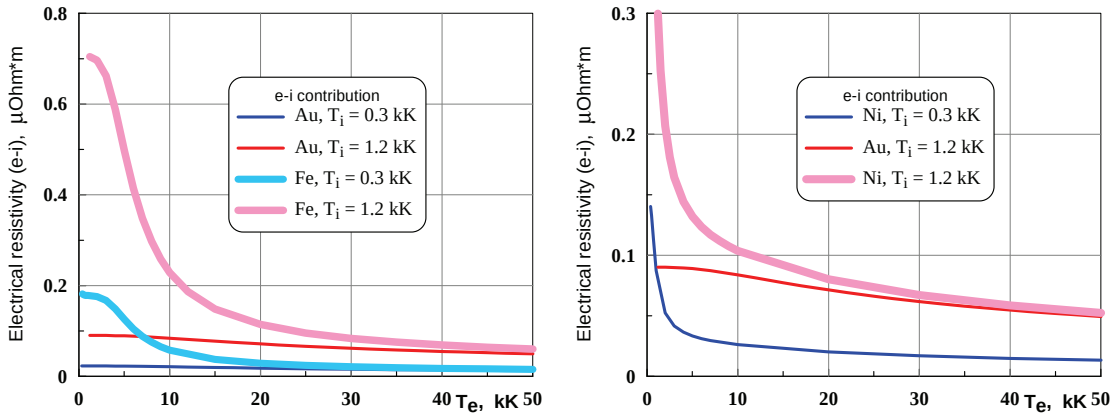

Figure 11. Resistivity σ of noble (Au) and transition metals (Fe, Ni) as functions of electron temperature T_e. *Left panel.* Comparison of functions $\sigma_{Au}(T_e)$ and $\sigma_{Fe}(T_e)$ at two fixed ion temperatures T_i =0.3 kK and 1.2 kK. *Right panel.* Nickel versus gold, qualitatively different behavior of resistivity.

In the integral for σ_d the electron energy is $\varepsilon' = \varepsilon_1 + p'^2/(2m_d)$, and it is convenient to change from the integration over p' to the integration over momentum of s-electron p with the help of relation (14). Then $p'dp' = m_0^2 pdp, \varepsilon' = \varepsilon = \varepsilon_s + \frac{p^2}{2m_s}$, and the range of integration over p is divided onto seven intervals shown above, only four of which contain momentum values, necessary to make it possible the scattering of d-electrons because of the quasielasticity of electron-phonon collisions.

By using calculated s- and d-electron conductivities, we can define effective frequencies of collisions of s- and d-electrons with phonons in dependence on two temperatures as those to give the same values of conductivities as obtained by the Drude formula:

$$\bar{\nu}_s = \frac{Z_s(T_e)ne^2}{m_s\sigma_s}, \qquad \bar{\nu}_d = \frac{Z_d(T_e)ne^2}{m_d\sigma_d}.$$

Here n is the concentration of atoms and Z_s and Z_d are the numbers of electrons per atom in s- and d-bands depending on electron temperature.

Relaxation times, calculated as the functions of electron momentum, also allow to calculate the electron heat conductivity coefficient. In the presence of electron temperature gradient deviation of the electron distribution function from its equilibrium value can be written in the form[20, 28]

$$f_1 = -\mathbf{v}\frac{\partial f_0}{\partial T_e}\tau(\varepsilon)\nabla T_e = \left(-\frac{\partial f_0}{\partial \varepsilon}\right)\left(\frac{\partial \mu}{\partial T_e} + \frac{\varepsilon-\mu}{\partial T_e}\right)\mathbf{v}\tau(\varepsilon)\nabla T_e$$

The density of electron heat flux at the temperature gradient directed along the z-axis is calculated as

$$\mathbf{q} = \int(\varepsilon-\mu)v_z f_1 2\frac{d^3p}{(2\pi\hbar)^3} = \int\left(-\frac{\partial f_0}{\partial \varepsilon}\right)\left(\frac{\partial \mu}{\partial T_e} + \frac{\varepsilon-\mu}{\partial T_e}\right)(\varepsilon-\mu)v_z^2\tau(\varepsilon)2\frac{d^3p}{(2\pi\hbar)^3}\frac{\partial T_e}{\partial z}$$

Whence electron heat conductivity coefficient is

$$\kappa = \frac{1}{3}\int\left(-\frac{\partial f_0}{\partial \varepsilon}\right)\left(\frac{\partial \mu}{\partial T_e} + \frac{\varepsilon-\mu}{\partial T_e}\right)(\varepsilon-\mu)v^2\tau(\varepsilon)2\frac{8\pi p^2 dp}{(2\pi\hbar)^3}$$

Electron heat conductivity coefficient due to the electron-phonon interaction is a sum of partial s-electron heat conductivity coefficient κ_s and d-electron heat conductivity coefficient κ_d: $\kappa = \kappa_s + \kappa_d$, as well as total electrical conductivity $\sigma = \sigma_s + \sigma_d$.

Resistivity as a function of the electron temperature at two values of ion temperatures $T_i = 0.3$ kK and $T_i = 1.2$ kK is shown in Fig. 11 for the noble metal (gold) and two transition metals (iron and nickel). We see

relatively small dependence of the resistivity of gold upon the electron temperature, while for transition metals the resistivity significantly drops with increase of electron temperature. Resistivity of nickel, having a Fermi level close to the upper edge of the electron d-band, drops faster than resistivity of iron with Fermi level lying more deeper inside the d-band.

ACKNOWLEDGMENTS

The work was supported by the Russian Foundation for Basic Research (project no. 13-02-01078).

REFERENCES

[1] Anisimov, S., Kapeliovich, B., and Perel'man, T., "Electron emission from metal surfaces exposed to ultrashort laser pulses," *Sov. Phys. JETP* **39**, 375–377 (1974).

[2] Elsayed-Ali, H. E., Juhasz, T., Smith, G. O., and Bron, W. E., "Femtosecond thermoreflectivity and thermotransmissivity of polycrystalline and single-crystalline gold films," *Phys. Rev. B* **43**, 4488–4491 (1991).

[3] Groeneveld, H. M., Sprik, R., and Lagendijk, A., "Femtosecond spectroscopy of electron-electron and electron-phonon energy relaxation in ag and au," *Phys. Rev. B* **51**(17), 11433–11445 (1995).

[4] Hohlfeld, J., Mueller, J. G., Wellershoff, S. S., and Matthias, E., "Time-resolved thermoreflectivity of thin gold films and its dependence on film thickness," *Appl. Phys. B* **64**(3), 387–390 (1997).

[5] Inogamov, N. A., Petrov, Y. V., Zhakhovsky, V. V., Khokhlov, V. A., Demaske, B. J., Ashitkov, S. I., Khishchenko, K. V., Migdal, K. P., Agranat, M. B., Anisimov, S. I., and Fortov, V. E., "Two-temperature thermodynamic and kinetic properties of transition metals irradiated by femtosecond lasers," *AIP Conf. Proc.* **1464**, 593–608 (2012).

[6] Petrov, Y. V., Inogamov, N. A., and Migdal, K. P., "Thermal conductivity and the electron-ion heat transfer coefficient in condensed media with a strongly excited electron subsystem," *JETP Lett.* **97**(1), 20–27 (2013).

[7] Petrov, Y. V. and Inogamov, N. A., "Elimination of the mott interband sd enhancement of the electrical resistance of nickel and platinum owing to the excitation of electrons by femtosecond laser pulses," *JETP Lett.* **98**(5), 278–284 (2013).

[8] Inogamov, N. A., Zhakhovsky, V. V., Petrov, Y. V., Khokhlov, V. A., Ashitkov, S. I., Khishchenko, K. V., Migdal, K. P., Ilnitsky, D. K., Emirov, Y. N., Shepelev, V. V., Oleynik, I. I., Agranat, M. B., Andriyash, A. V., Anisimov, S. I., and Fortov, V. E., "Electron-ion relaxation, phase transitions, and surface nanostructuring produced by ultrashort laser pulses in metals," *Contrib. Plasma Phys.* **X**(X), 1–15 (2013).

[9] Mueller, B. Y. and Rethfeld, B. *Phys. Rev. B* **87**, 035139 [12 pages] (2013).

[10] Lin, Z., Zhigilei, L. V., and Celli, V., "Electron-phonon coupling and electron heat capacity of metals under conditions of strong electron-phonon nonequilibrium," *Phys. Rev. B* **77**, 075133 (2008).

[11] Kresse, G. and Furthmuller, J., "Efficiency of ab initio total energy calculations for metals and semiconductors using a plane-wave basis set," *Computational Materials Science* **6**(1), 15–50 (1996).

[12] Sin'ko, G. V. and Smirnov, N. A., "Ab initio calculations of the equation of state and elastic constants of aluminum in the region of negative pressures," *JETP Lett.* **75**(4), 184–186 (2002).

[13] Sin'ko, G. V., Smirnov, N. A., Ovechkin, A. A., Levashov, P. R., and Khishchenko, K. V., "Thermodynamic functions of the heated electron subsystem in the field of cold nuclei," *High Energy Density Physics* **9**, 309–314 (2013).

[14] Recoules, V., Clerouin, J., Zerah, G., Anglade, P. M., and Mazevet, S., "Effect of intense laser irradiation on the lattice stability of semiconductors and metals," *Phys. Rev. Lett.* **96**, 055503 (2006).

[15] Khakshouri, S., Alfe, D., and Duffy, D. M., "Development of an electron-temperature-dependent interatomic potential for molecular dynamics simulation of tungsten under electronic excitation," *Phys. Rev. B* **78**, 224304 (2008).

[16] Loboda, P. A., Smirnov, N. A., Shadrin, A. A., and Karlykhanov, N. G., "Simulation of absorption of femtosecond laser pulses in solid-density copper," *High Energy Density Physics* **7**(4), 361–370 (2011).

[17] Chen, Z., Holst, B., Kirkwood, S. E., Sametoglu, V., Reid, M., Tsui, Y. Y., Recoules, V., and Ng, A., "Evolution of ac conductivity in nonequilibrium warm dense gold," *Phys. Rev. Lett.* **110**(13), 135001 (2013).

[18] Norman, G., Saitov, I., Stegailov, V., and Zhilyaev, P., "Atomistic modeling and simulation of warm dense matter. conductivity and reflectivity," *Contributions to Plasma Physics* **53**(4-5), 300–310 (2013).
[19] Knyazev, D. V. and Levashov, P. R., "Ab initio calculation of transport and optical properties of aluminum: Influence of simulation parameters," *Computational Materials Science* (in press).
[20] Abrikosov, A. A., [*Introduction to the Theory of Normal Metals*], NY: Academic Press (1972).
[21] Inogamov, N. A. and Petrov, Y. V., "Thermal conductivity of metals with hot electrons," *JETP* **110**(3), 446–468 (2010).
[22] Recoules, V. and Crocombette, J., "Ab initio determination of electrical and thermal conductivity of liquid aluminum," *Phys. Rev. B* **72**, 104202 (2005).
[23] Sha, X. and Cohen, R. E., "First-principles studies of electrical resistivity of iron under pressure," *J. Phys.: Condens. Matter* **23**, 075401 (2011).
[24] Alfe, D., Pozzo, M., and Desjarlais, M. P., "Lattice electrical resistivity of magnetic bcc iron from first-principles calculations," *Phys. Rev. B* **85**, 024102 (2012).
[25] Norman, G. E., Starikov, S. V., Stegailov, V. V., Saitov, I. M., and Zhilyaev, P. A., "Atomistic modeling of warm dense matter in the two-temperature state," *Contrib. Plasma Phys.* **53**(2), 129–139 (2013).
[26] Zhilyaev, P. A., Norman, G. E., and Stegailov, V. V., "Ab initio calculations of thermal conductivity of metals with hot electrons," *Doklady Physics* **58**(8), 334–338 (2013).
[27] Mott, N. F., "The electrical conductivity of transition metals," *Proc. R. Soc. Lond. A* **153**, 699–717 (1936).
[28] Blatt, F. J., [*Physics of electronic conduction in solids*], McGrow-Hill Book Company (1968).